forum acusticum 2026
8-12 September · Graz, Austria

INFLUENCE OF THE SPOT SIZE IN TRANSIENT GRATING SPECTROSCOPY

Jakub Kušnír[1,2], Zbyněk Makovský[3], Tomáš Grabec[1], David Mareš[1], Kristýna Repček[2], Pavla Stoklasová[1], Petr Sedlák[1], Hanuš Seiner[1]

[1] *Institute of Thermomechanics of the Czech Academy of Sciences, Prague, Czechia*
[2] *Faculty of Nuclear Sciences and Physical Engineering, Czech Technical University in Prague, Prague, Czechia*
[3] *Grammar school Pardubice Dašická 1083, Pardubice, Czechia*

This paper is a revised version of the authors' submitted manuscript that was peer-reviewed by at least two anonymous reviewers.

Abstract

The influence of spot size on the quality of the time- and frequency-domain results of transient grating spectroscopy (TGS) was investigated. The experiment was performed on a single-crystalline sample of Ni with a highly symmetrical cut (110). Sharpening of the frequency peaks of the SAW was observed for larger spot sizes. However, the best obtainable sharpness of the frequency peaks strongly depends on the crystallographic direction of the propagating SAW. Furthermore, ultra-transient effects observable in UTGS measurements depended strongly on the power density of the pump laser.

Keywords: *transient grating spectroscopy, elastic anisotropy, surface acoustic waves, single-crystals*

1. Introduction

Transient grating spectroscopy (TGS) is a non-destructive and contactless opto-acoustic technique used to characterize the elastic and thermal properties of materials [1], [2], [3]. In a reflective geometry used for opaque solids, TGS was used to determine the elastic properties of single-crystalline [3], [4], poly-crystalline samples [5], [6], and thin-films [7], [8], [9], as well as martensitic transformation [10], irradiation effects [11], [12], [13], and thermal diffusivity [14], [15]. Recently, the existence of ultra-transient features was described as the ultra-transient grating spectroscopy (UTGS) approach [16], leading to experimental reconstruction of elastodynamic frequency-domain Green's function of the surface acoustic response [17].

TGS uses two pulsed laser beams interfering on the sample surface, which results in the spatially harmonic thermo-elastic excitation, where each of the excitation fringes acts as a thermo-elastic line-like source. This leads to a strong constraint on the spatial characteristics of the surface thermo-acoustic source, forming dynamic surface-displacement grating on which the probe beams diffract. The probe laser is continuous, and the optical geometry ensures recombination of the probe beams in a heterodyne detection setup [1]. The relative phase shift of the probe beams (the heterodyne phase) then influences the information obtained. The 'phase-grating' mode with the heterodyne phase $\theta_{\text{het}} = (\pm\pi/2)$ allows us to measure thermal and elastic properties simultaneously [2], [15], [18].

Most analytic treatments assume an infinite, uniform grating, [18], [19], [20] but real experiments use finite, typically Gaussian, pump and probe beams. Despite routine consideration of grating period and beam overlap in experimental design, the influence of finite spot sizes—through effects such as beam diffraction, Gaussian envelope truncation, spatial averaging of dynamics, and non-uniform excitation densities—has been the subject of comparatively few systematic studies. A notable exception is Dryburgh et al. [21], who examined the influence of the number of excitation fringes and measurement averages on the SAW standard deviation.

This paper examines how the sizes of pump and probe spots—with a fixed 2:1 size ratio, but varying absolute size—influence the quality of the TGS signal in the time- and frequency-domains for a single-crystalline sample with elastic anisotropy.

2. Methods - Transient Grating Spectroscopy

Transient grating spectroscopy in reflective geometry, illustrated in Fig. 1, uses a transmission phase mask for a diffraction of pump and probe lasers and projecting ±1 diffraction order beams on the sample surface using the 4F imaging system. Projected pump beams

***Corresponding author**: kusnir@it.cas.cz.*

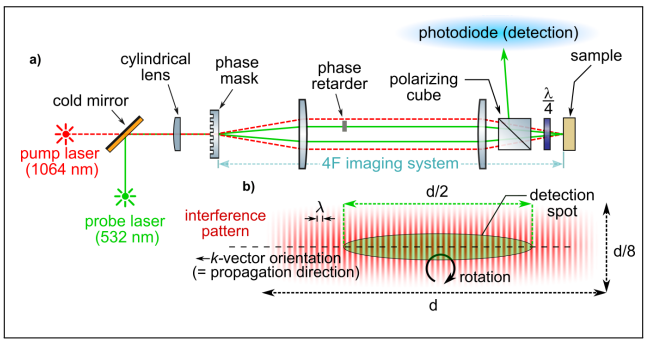

Figure 1: a) Top-view schematic of the simplified optical setup of the TGS method. b) Interference pattern with a fixed 2:1 pump-to-probe size ratio. Cylindrical lens is used to create a highly-elliptical spot for both pump and probe.

interfere on the sample surface, creating a spatially harmonic excitation pattern. The harmonic pattern leads to the formation of thermal and acoustic transient gratings, on which the probe beams are diffracted. A fixed 2:1 pump-to-probe beam diameter ratio is maintained throughout the discussed measurements. A cylindrical lens is used to create a highly-elliptical spot for both lasers to have higher energy density within the pattern while maintaining larger number of wavelengths. The optical setup is in the Littrow configuration, where each probe beam diffracts in the reflection direction of the other, enabling interferometric ('heterodyne') detection. Detection is carried out in the 'phase-grating' mode (with the heterodyne phase $\theta_{\text{het}} = (\pm\pi/2)$), which maximizes sensitivity to out-of-plane displacement.

The measurement setup was similar to that used in the previous work of the authors [3]. The pump laser was a Nd:YAG laser (1064 nm, 0.54 ns, 200 µJ, 1 kHz). The probe beams were from the continuous-wave laser at 532 nm (120 mW) with mean power on detector around 15 mW for all measurements. The signal-to-noise ratio and sensitivity are increased by measuring the intensity using Si photodiodes with a 60 dB amplifier. The differential setup further enhances the signal quality by removing phase-insensitive influences [18], [22].

The signal was recorded by WaveRunner 640Zi oscilloscope (4 GHz bandwidth, vertical resolution of 8 bits, sampling rate 5 GS /s) and averaged 50,000 times in the time-domain for further reduction of noise. The Fourier analysis then reveals the dominant SAW frequencies, from which the SAW velocities were obtained using $v = f\lambda$, where λ is the excitation grating period.

The fringe spacing, and thus the acoustic wavelength λ, is determined by the period d_{PM} of the phase mask and the magnification M of the 4F imaging system. For normal incidence on the phase mask, the diffraction condition $\sin(\theta/2) = \lambda_{\text{opt}}/d_{PM}$ causes the optical wavelength to cancel, giving:

$$\lambda = \frac{d_{PM}}{2M}, \tag{1}$$

where θ is the angle between the two excitation beams [23]. When holding the normal incidence (disregarding the phase-mask tilting [23]), the acoustic wavelength can therefore be changed by swapping the phase mask (changing d_{PM}) or by changing the lenses in the 4F imaging system (changing M)—which, however, affects the pattern size at the sample.

Table 1: Phase mask used in the measurement with a corresponding focal length ratio used in the 4F imaging system. The effective pump spot size was determined from the oscillation time of Ni(110)[100].

Phase mask (µm)	f1:f2	Pump (µm)
20	2:1	≈ 450
10	1:1	≈ 900
5	1:2	≈ 1800

3. Results and Discussion

The sample used in this study was a nickel single-crystal with cubic symmetry and Zener anisotropy ratio $Z = 2.6$. The principal cut, (110) in Miller indices, was chosen as this allows comparison of highly-symmetrical directions, like [100], with more arbitrary direction in the (110) plane.

Three measurements configurations were performed, each combining a different phase mask period d_{PM} and 4F imaging system magnification M such that the acoustic wavelength λ remained ≈ 10 µm in all cases, while the effective pump spot size varied from 450 µm to 1800 µm (Table 1). The power of the probe beams was constant for all measurements. For the largest and middle spot sizes, the pump beam average power was kept the same; for the smallest spot, it was reduced to avoid surface ablation.

3.1. Time-domain signal and effective spot size

The comparison of the obtained time-domain signals in the chosen crystallographic direction is shown in Fig. 2. We can observe that for the angle 0°—corresponding to [100] direction—the time of the oscillations scales linearly with a spot size. This is expected in principal direction on a single-crystalline sample, the SAW oscillation lifetime corresponds directly to the pattern size (or more precisely, to the number of wavelengths within it) as it avoids any influences of elastic anisotropy [3]. Thus, the effective pump spot size noted in Table 1 was determined from the oscillation time in this direction.

However, for the angle 30°, the SAW lifetime is notably shorter, with much lower correlation to the spot size—there is only a small increase in oscillation time between the smallest and middle size spots and no difference between the largest and middle size spots. This

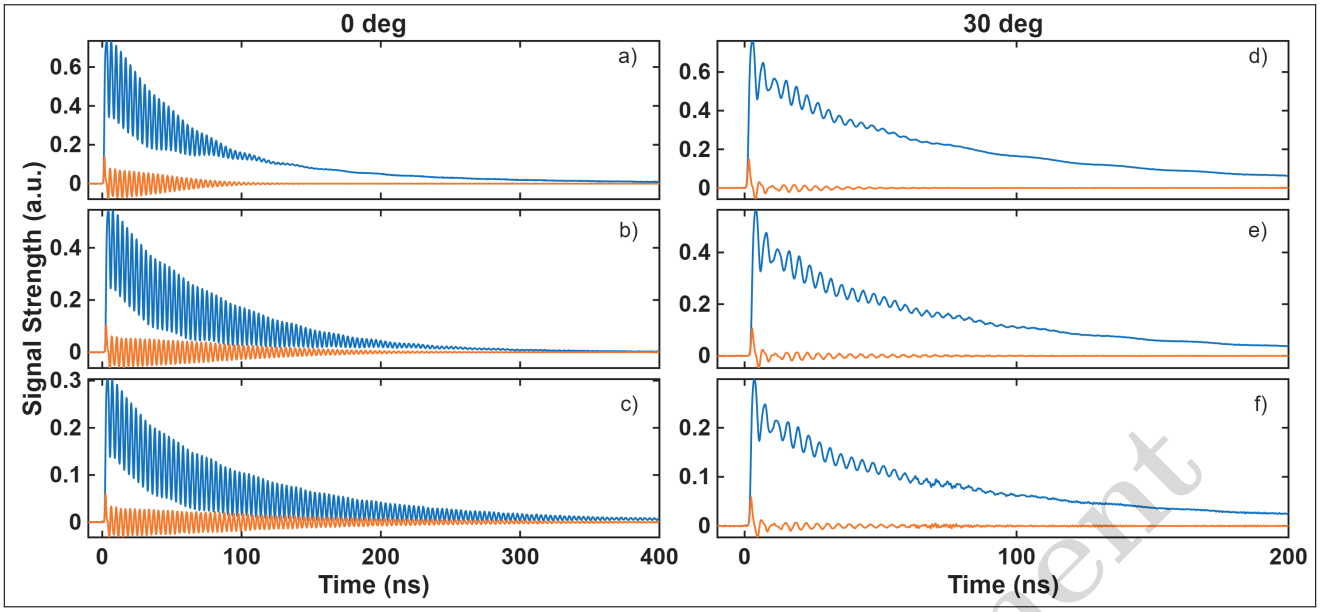

Figure 2: Comparison of the TGS time-domain signals in Ni(110)[100] as angle 0° (a, b and c) and angle 30° (d, e and f). Measured signals in solid blue and numerical derivation of measured signals in solid orange to better show differences in acoustic oscillations. Top row represent smallest spot size, middle row the middle size, and bottom row largest spot size described in Table 1.

is likely due to the elastic anisotropy, which causes the SAW to be of more complex polarization (with lower out-of-plane component), and introduces energy steering (meaning that SAWs generated farther from the probing spot can miss it and avoid being detected). The optimal spot size for the longest oscillation time therefore depends on the crystallographic directions.

3.2. Angular-resolved velocity maps

For all 4F system configurations—and thus different pattern sizes—the full angular dispersion was measured in the range of 90°, with a step of 1°. Comparison of the resulting angular-resolved velocity maps in Fig. 3 (showing frequency spectra recalculated to velocity as $v = f\lambda$) shows sharpening of the SAW peaks near principal directions—[001] at 0°, [1$\bar{1}$1] near 60°, and [0$\bar{1}$1] at 90°—with larger spot sizes. Away from these directions, the difference lowers, corresponding to the decreasing influence of spot size to the lifetime of the oscillations shown in Fig. 2d-f.

This is better illustrated in Fig. 4, which compares the relative amplitude of the SAW peak with respect to the reference amplitude of the shear-wave shoulder at 30°—the exact reference value was obtained by taking the mean amplitude between 3.0 and 3.4 um/ns.

Figure 3 d) shows a calculated elastodynamic surface frequency-domain Green's function [17], which is the response to a spatially harmonic source, and thus represents the idealized infinite-spot limit. The correspondence to the measured signals shows that the ultra-transient features—finer features in the spectra connected to bulk waves, which are observed only in a short time after the excitation [16]—are clearly better resolved for the middle spot size than for the smallest one. However, their resolution does not improve for the largest spot size, which is consistent with the fact that the middle and the largest spots had the same total pump power, leading to different power densities. This suggests that the quality of these features is governed by the pump power density within the pattern rather than simply by the pattern size.

4. Conclusion

In this work, we present the results of spot-size modifications on the resulting data quality of the TGS measurement. For principal crystallographic directions, increased spot size produces longer SAW oscillation lifetimes and correspondingly sharper peaks in the frequency domain. However, the improvement depends on the crystallographic direction — and little to no influence of spot size can be found in directions where the generalized surface wave has a low out-of-plane displacement component, or where its energy steers away from the k-vector direction given by the pattern (and the counter-propagating waves do not meet in the detection spot). The amplitude of ultra-transient features depends on the power density within the excitation pattern. Their prominence above noise, while expected to improve with larger pattern size, requires further study with varying pump pattern parameters and pump-to-probe spot size ratios.

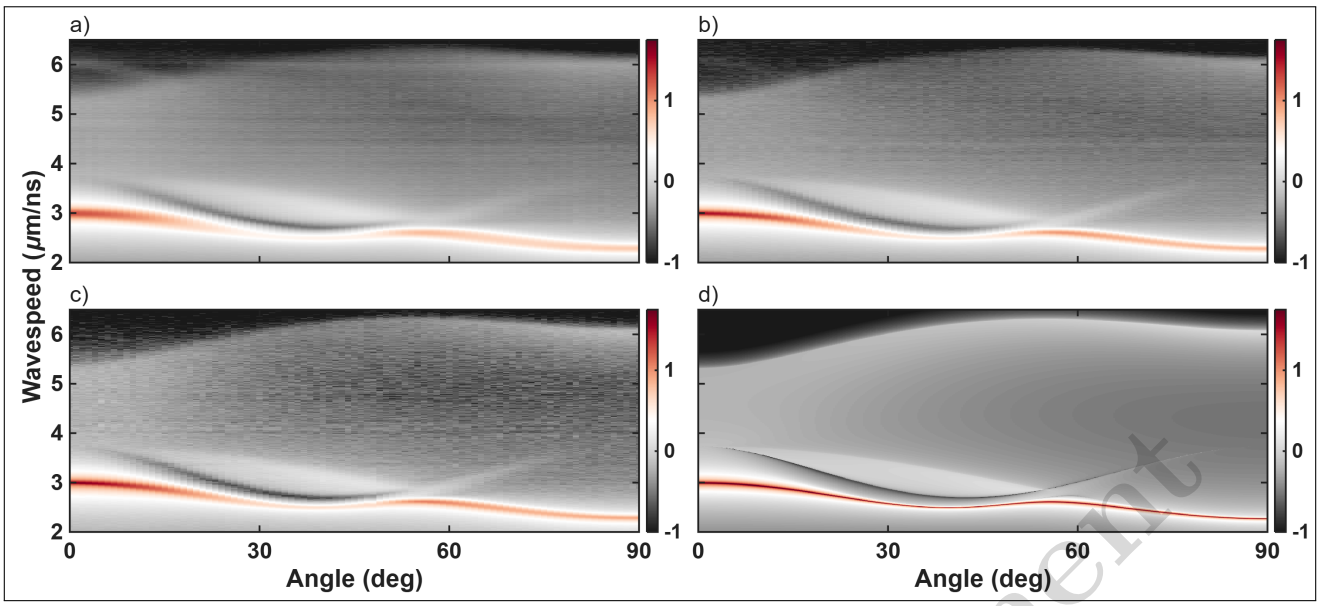

Figure 3: Comparison of TGS angular-resolved velocity maps—(a,b,c) for the smallest, middle, and largest spot, respectively—with the calculated frequency-domain Green's function (d). For all maps (a,b,c and d), a reference amplitude was taken as that of the shear-wave shoulder at 30°, and the colorbar then shows the logarithmic ratio of the frequency-domain amplitude and the reference amplitude (with the reference amplitude corresponding to the value of 0) — note how the peak prominence and sharpening given by the relative coloring differs (in logarithmic scale).

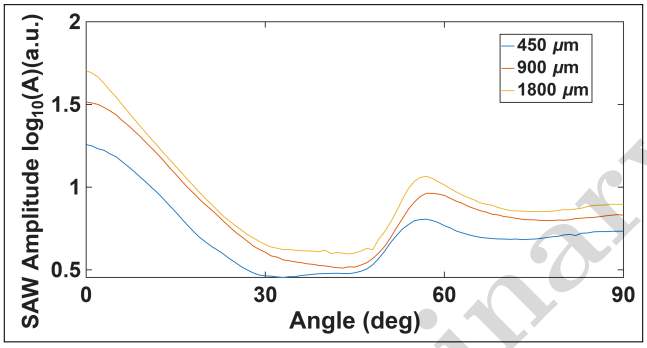

Figure 4: Comparison of the SAW peak relative amplitude normalized to the shear-wave shoulder at 30°, showing how the larger spot size (yellow) corresponds to more prominent SAW peak near principal directions (0, 60, and 90 degrees) compared to the smaller spot sizes, while the difference lowers away from these directions. Note that, due to the logarithmic scale, the shear-wave shoulder corresponds to $log_{10}(A) = 0$.

5. Acknowledgments

This work was financially supported by Czech Science Foundation [Project No. 24-10366S], Operational Program Johannes Amos Comenius of the Ministry of Education, Youth and Sport of the Czech Republic, within the frame of project Ferroic Multifunctionalities (FerrMion) [Project No.CZ.02.01.01/00/22_008/0004591], co-funded by the European Union and by the Grant Agency of the Czech Technical University [No. SGS25/168/OHK4/3T/14].

References

[1] A. A. Maznev, K. A. Nelson, and J. A. Rogers, "Optical heterodyne detection of laser-induced gratings," *Opt. Lett.*, vol. 23, no. 16, pp. 1319–1321, 1998. DOI: 10.1364/OL.23.001319.

[2] J. A. Johnson et al., "Phase-controlled, heterodyne laser-induced transient grating measurements of thermal transport properties in opaque material," *Journal of Applied Physics*, vol. 111, no. 2, p. 023 503, 2012. DOI: 10.1063/1.3675467.

[3] P. Stoklasová, T. Grabec, K. Zoubková, P. Sedlák, S. Krátký, and H. Seiner, "Laser-Ultrasonic Characterization of Strongly Anisotropic Materials by Transient Grating Spectroscopy," *Experimental Mechanics*, 2021. DOI: 10.1007/s11340-021-00698-6.

[4] K. Repček et al., "Compliant Lattice Modulations Enable Anomalous Elasticity in Ni–Mn–Ga Martensite," *Advanced Materials*, vol. 36, no. 39, p. 2 406 672, 2024. DOI: 10.1002/adma.202406672.

[5] A. Reza et al., "Non-contact, non-destructive mapping of thermal diffusivity and surface acoustic wave speed using transient grating spectroscopy," *Review of Scientific Instruments*, vol. 91, no. 5, p. 054 902, 2020. DOI: 10.1063/5.0003742.

[6] C. Weaver, M. Stapelberg, M. P. Short, A. Wylie, and E. B. Artalejo, "Automated transient grating spectroscopy mapping and signal control for

large samples," *Review of Scientific Instruments*, vol. 95, no. 7, p. 074 902, 2024. DOI: 10.1063/5.0202262.

[7] J. A. Rogers, A. A. Maznev, M. J. Banet, and K. A. Nelson, "Optical Generation and Characterization of Acoustic Waves in Thin Films: Fundamentals and Applications," *Annual Review of Materials Science*, vol. 30, no. 1, pp. 117–157, 2000. DOI: 10.1146/annurev.matsci.30.1.117.

[8] J. Sermeus, R. Sinha, K. Vanstreels, P. M. Vereecken, and C. Glorieux, "Determination of elastic properties of a MnO2 coating by surface acoustic wave velocity dispersion analysis," *Journal of Applied Physics*, vol. 116, no. 2, p. 023 503, 2014. DOI: 10.1063/1.4885427.

[9] T. Grabec et al., "Guided acoustic waves in thin epitaxial films: Experiment and inverse problem solution for NiTi," *Ultrasonics*, vol. 138, 2024. DOI: 10.1016/j.ultras.2023.107211.

[10] T. Grabec et al., "In-situ Characterization of Local Elastic Properties of Thin Shape Memory Films by Surface Acoustic Waves," *Smart Materials and Structures*, vol. 25, no. 12, 2016. DOI: 10.1088/0964-1726/25/12/127002.

[11] F. Hofmann, M. P. Short, and C. A. Dennett, "Transient grating spectroscopy: An ultrarapid, nondestructive materials evaluation technique," *MRS Bulletin*, vol. 44, no. 5, pp. 392–402, 2019. DOI: 10.1557/mrs.2019.104.

[12] E. Trachanas et al., "Thermal diffusivity variation assessment on Radio-Frequency Quadrupole Cu-OF copper due to proton irradiation," *Nuclear Instruments and Methods in Physics Research Section B: Beam Interactions with Materials and Atoms*, vol. 539, pp. 179–189, 2023. DOI: 10.1016/j.nimb.2023.04.002.

[13] A. Shamatova et al., "Anisotropic thermal transport in robust crystalline yttrium aluminium garnet tunable by long oriented amorphous nanotracks," *International Journal of Thermal Sciences*, vol. 222, p. 110 583, 2026. DOI: 10.1016/j.ijthermalsci.2025.110583.

[14] J. A. Johnson et al., "Direct Measurement of Room-Temperature Nondiffusive Thermal Transport Over Micron Distances in a Silicon Membrane," *Physical Review Letters*, vol. 110, no. 2, p. 025 901, 2013. DOI: 10.1103/PhysRevLett.110.025901.

[15] C. A. Dennett and M. P. Short, "Thermal diffusivity determination using heterodyne phase insensitive transient grating spectroscopy," *Journal of Applied Physics*, vol. 123, no. 21, p. 215 109, 2018. DOI: 10.1063/1.5026429.

[16] T. Grabec et al., *Ultra-transient grating spectroscopy for visualization of surface acoustics*, 2025. DOI: 10.48550/arXiv.2510.10696.

[17] A. G. Every, K. Y. Kim, and A. A. Maznev, "The elastodynamic response of a semi-infinite anisotropic solid to sudden surface loading," *The Journal of the Acoustical Society of America*, vol. 102, no. 3, pp. 1346–1355, 1997. DOI: 10.1121/1.420053.

[18] O. W. Käding, H. Skurk, A. A. Maznev, and E. Matthias, "Transient thermal gratings at surfaces for thermal characterization of bulk materials and thin films," *Applied Physics A*, vol. 61, no. 3, pp. 253–261, 1995. DOI: 10.1007/BF01538190.

[19] J. Kušnír, T. Grabec, K. Zoubková, P. Stoklasová, P. Sedlák, and H. Seiner, "Apparent anisotropic thermal diffusivity measured in cubic single crystals by transient grating spectroscopy," *Journal of Applied Physics*, vol. 133, no. 12, p. 125 108, 2023. DOI: 10.1063/5.0136850.

[20] J. Kušnír, T. Grabec, P. Sedlak, P. Stoklasová, and H. Seiner, "Study of the acoustic and thermal response of an elastically anisotropic solid to a sub-nanosecond laser pulse in transient grating spectroscopy," *Modelling and Simulation in Materials Science and Engineering*, 2026. DOI: 10.1088/1361-651X/ae5676.

[21] P. Dryburgh et al., "Measurement of the single crystal elasticity matrix of polycrystalline materials," *Acta Materialia*, vol. 225, p. 117 551, Feb. 2022, ISSN: 1359-6454. DOI: 10.1016/j.actamat.2021.117551. Accessed: Jul. 16, 2026. [Online]. Available: https://www.sciencedirect.com/science/article/pii/S1359645421009290.

[22] B. Verstraeten, J. Sermeus, R. Salenbien, J. Fivez, G. Shkerdin, and C. Glorieux, "Determination of thermoelastic material properties by differential heterodyne detection of impulsive stimulated thermal scattering," *Photoacoustics*, vol. 3, no. 2, pp. 64–77, 2015. DOI: 10.1016/j.pacs.2015.05.001.

[23] A. Vega-Flick et al., "Laser-induced transient grating setup with continuously tunable period," *Review of Scientific Instruments*, vol. 86, no. 12, p. 123 101, 2015. DOI: 10.1063/1.4936767.